Contents list available at CBIORE journal website

International Journal of Renewable Energy Development

Journal homepage: https://ijred.cbiore.id

Research Article

Multi-objective optimisation and sensitivity analysis of component influences on efficiency in air-based bifacial photovoltaic thermal systems (B-PVT)

Ahmad Rajani[a,b,c], Dalila Mat Said[a,c*], Zulkarnain Ahmad Noorden[a], Nasarudin Ahmad[a], Muhammad Subhan Arifin[d], Udin Komarudin[e], Tinton Dwi Atmaja[a,b,c], Subagyo[b], Ahmad Fudholi[b,f]

[a]*Faculty of Electrical Engineering, Universiti Teknologi Malaysia, Johor, Malaysia*

[b]*Research Centre for Energy Conversion and Conservation, BRIN, Serpong, Indonesia*

[c]*Centre of Electrical Energy System (CEES), Institute of Future Energy, UTM, Johor, Malaysia*

[d]*Faculty of Mechanical and Aerospace Engineering, Institut Teknologi Bandung, Indonesia*

[e]*Mechanical engineering, Faculty of Engineering, Widyatama University, Indonesia*

[f]*Solar Energy Research Institute, Universiti Kebangsaan Malaysia, 43600 Bangi Selangor, Malaysia*

Abstract. Bifacial Photovoltaic Thermal (B-PVT) technologies have seen significant advancements in sustainable energy production by converting solar energy into useful electric and thermal energies simultaneously. The present study explored the optimisation of these systems by first performing sensitivity analysis on design parameters to identify key variables affecting their performance efficiencies. The system design and performance were then studied simultaneously using a multi-objective optimisation algorithm NSGA-II. It was found that increasing packing factors from 0.4 to 0.8 leads to a 15% increase in both electrical and thermal efficiencies, while an asymmetry in channel depths could lead to an 8% increase in thermal efficiency. Key design parameters such as transmissivity cover, mass flow rate, packing factors and channel depth ratios were found to have the most significant influence on overall system performance. Multi-objective optimisation of design variables results in a Pareto front describing trade-offs between solutions of conflicting objectives of performance. Optimisation with preferences towards overall efficiency over temperature differential produces solutions with a high overall efficiency yield of 70.79%, requiring specific values for mass flow rate (0.197 kg/s) and channel ratio (0.129), however at the expense of a reduced temperature differential of 5.12°C. Solutions with a balanced preference towards both objectives could produce a solution that is less biased in performance.

Keywords: Bifacial Photovoltaic Thermal (B-PVT), Multi-Objective Optimization, NSGA-II, Efficiency Enhancement, Sensitivity Analysis.

Received: 27th March 2024; Revised: 16th May 2024; Accepted: 29th May 2024; Available online: 14th June 2024

1. Introduction

In recent years, the over-reliance on the use of fossil fuels for energy has resulted in significant environmental issues due to increased greenhouse emissions into the atmosphere (Su *et al.*, 2022), increasing the need for much cleaner energy production. Solar energy has been arguably regarded as a viable, sustainable solution due to its abundance and renewable nature, a favourable trait given the current state of global warming and pollution (Rajani *et al.*, 2018; Urrejola *et al.*, 2016). The advancement of Photovoltaic Thermal (PVT) technology, therefore, stands out as one of the myriads of potential solutions which could harness solar power to generate useable energies. A particular advantage of this technology is its ability to generate both electrical and thermal energies (Nazri *et al.*, 2019), resulting in high levels of efficiency. In easing the transition into renewable energy sources, optimisation of these PVT systems becomes of interest in order to realise their full potential for sustainable energy generation.

In increasing the performance efficiencies of these PVT systems, researchers have explored various configurations, primarily with a focus on the working fluid as its heat transfer media. These fluids may be in the form of air (Abdulmajeed *et al.*, 2022; Choi 2022), water (Hamada *et al.*, 2023; Abdul-Ganiyu *et al.*, 2021) or nanofluids (Zarei *et al.*, 2023; Youns and Manshad 2023). Detailed investigations on the fluid dynamics within these PVT systems in relation to their performance often involve varying its mass flow velocities through the system. A study

* Corresponding author
Email: dalila@utm.my (D.M.Said)

https://doi.org/10.61435/ijred.2024.60212
ISSN: 2252-4940/© 2024.The Author(s). Published by CBIORE

performed by (Podder *et al.,* 2023) on a water-based PVT system found improved electrical and thermal efficiencies, reaching a maximum of 89.96% and 11.47%, respectively, by increasing the mass flow rate from 0.004 to 0.08 kg/s. Additional studies conducted by (Tiwari *et al.,* 2023a) found similar trends in PVT systems with nanofluids improving both overall and electrical efficiencies by around 10% when increasing its mass flow rate from 0.05 to 0.2 kg/s.

Further performance optimisation has been extended to investigations on reflector shapes within the PVT systems with the investigation on the usage of V-grove mirror reflectors in bifacial photovoltaic thermal (B-PVT) systems (Mustapha *et al.,* 2023). Additional studies on spiral-shaped (Ranjan *et al.,* 2023) and triangle-shaped reflectors (An, Choi, and Choi, 2022) have also been performed, each with its performance benefits. A B-PVT system utilises bifacial photovoltaic (PV) cells enabling both its faces for energy harvesting, thus increasing its local electric generation. Solar irradiation, which penetrates through the bifacial PV cells, is reflected onto the second face, generating increased electrical output than monofacial PV cells. As the PV cells heat up during operation, their thermal energy is transferred away, facilitated by heat transfer media such as air (Gopi and Muraleedharan, 2022), offering additional benefits, including indirect solar drying and optimal temperature regulation for the cooling of the PV cells.

Packing factors (PF), denoting the ratio between the total area of PV cells to the total area of its module of B-PVT systems, is one of the important factors that affect the system's performance. (Ishak *et al.,* 2023) examined efficiencies yielded via a parameter sweep of packing factors: 0.22, 0.33 and 0.66, where it was found that higher packing factors result in its highest thermal efficiency of 61.43%. Similar results were found in other independent studies on B-PVT systems, where its highest exergy efficiency had a relatively higher PF (Ewe *et al.,* 2023). However, there has yet been extensive research which delved in-depth into simultaneously optimising other relevant factors pertaining to B-PVT systems to maximise its output performance. In light of this, the present study investigates the potential performance improvements of B-PVT systems.

Multi-objective optimisation is a common approach used by researchers in systematically identifying system configurations and states of each of their components, providing the relevant mechanical and physical phenomena can be mathematically modelled and a performance objective can be formulated. For instance, (Li *et al.,* 2019) have implemented a multi-objective optimisation framework for optimal performance on earth-air heat exchangers (EAHE) and building-integrated photovoltaic/thermal (BIPVT) system configurations to great effect, while other researchers have taken an interest in the multi-objective optimisation of performance parameters for other types of PVT collectors (J. Tamayo Vera, Laukkanen, and Sirén 2014; Kallio and Siroux 2020). One main advantage of a multi-objective approach is the assurance of a set of optimal results provides users with solutions that infer information on the trade-off relationship between conflicting objectives. These solutions could then be chosen based on the user's preferences and requirements.

Design parameters factoring into the PVT output efficiencies have since been thoroughly studied and examined in various available literature reviews. However, there is still a significant shortcoming in the existing literature that has explicitly tackled the performance optimisation of air-based B-PVT systems with respect to their system components and configurations. Furthermore, an analysis of the effects of each of their design parameters on the overall system characteristic performance has yet been performed. This study aims to contribute to the advancement of PVT collectors by first conducting a sensitivity analysis on air-based B-PVT systems to investigate each component's influences towards the performance output. The results of the sensitivity analysis would then help in reducing the number of decision variables for optimisation to those parameters that only have significant effects on the performance objective. This process is essential in reducing the computational power needed in the multi-objective optimisation process of the B-PVT system.

The present study developed a mathematical model of the B-PVT system, based on heat transfer relations, to serve as a surrogate model for the real-world B-PVT system. This mathematical model was validated and was then used for optimisation. A metaheuristic multi-objective optimisation algorithm framework, namely NSGA-II, was implemented to find optimal solutions of output performance where each solution provides optimal performance, each with the distinct configurations of its system components. The objectives of the studies include developing a valid model of the B-PVT system and conducting a sensitivity analysis to better understand the significance of each component towards the performance objectives. In this study, the performance objective chosen is the system's electrical (η_{pv}) and thermal efficiencies (η_{th}), as well as its temperature differential (ΔT). The use of an elitist NSGA-II multi-objective algorithm offers multiple solutions and infers information on B-PVT characteristics. Each solution balances the different preferences towards conflicting objectives to be chosen based on preferences and design requirements of the use. This research aims to provide insights to be used as points of reference for future B-PVT advancements.

2. Methodology

The research methodology was approached as outlined in Figure 1. An initial phase of developing a mathematical model of the Bifacial-Photovoltaic Thermal (B-PVT) based on heat transfer modes along with its design parameter variables was carried out, followed by its validation using experimental data under continuously varying conditions. Sensitivity analysis was then conducted to identify the various design parameters that have significant affects towards the performance efficiencies. A multi-objective optimisation procedure, with two-(2D) and three-(3D) conflicting objectives, was studied for in-depth analysis. The 2D resulted in an analysis which provides an examination of the relationship between only two different objectives, offering a more detailed insight. Simultaneously, the 3D resulted in an analysis that enables the exploration of relationships between all three objectives. Each optimal solution produced by the optimisation was expected to yield distinct optimal solutions, each with different preferences towards different objectives.

2.1 B-PVT mathematical model

The nominal design configuration concept of the B-PVT collector used in the present study is illustrated in Figure 2, where the heat transfer media, air, passed through the first channel before getting redirected through the second channel. This configuration is known as a “double-pass system”. Double-pass systems have been previously investigated on thermal energy storage units (TES) (Gürbüz *et al.,* 2023), and comparisons have been made against a single-pass system (Gopi and Muraleedharan, 2022). It was found that a double-pass system offers greater thermal energy transfer capabilities and consequently provides greater cooling effects to the bifacial PV cells, as a double-pass system doubles the surface area in contact with the cells.

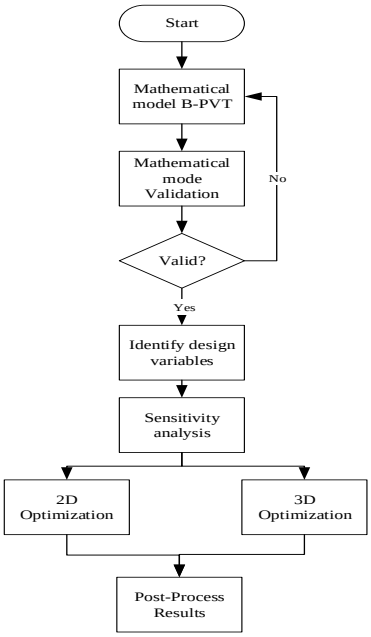

Fig. 1 Flow chart of the research process.

a. Energy balance equation

In interpreting the heat transfer phenomenon present in the B-PVT system, energy balance equations are required. Under the assumption of steady-state conditions and taking into account the relevant heat transfer coefficients, the energy balance equations (1) through (5) are written as follows:

B-PVT cover

$$\alpha_g I = U_t(T_g - T_{amb}) + h_{cgf1}(T_g - T_{f1}) - h_{rLg}(T_{pv} - T_g) \quad (1)$$

Airflow in the upper channel

$$(2\dot{m}C/WL)T_{in} = h_{cgf1}(T_g - T_{f1}) + h_{cLf1}(T_{pv} - T_{f1}) \quad (2)$$

Bifacial PV laminate

$$I_{pv} = h_{cLf1}(T_{pv} - T_{f1}) + h_{cLf2}(T_{pv} - T_{f2}) + h_{rLg}(T_{pv} - T_g) - h_{rLR}(T_{pv} - T_R) \quad (3)$$

Airflow in the lower channel

$$\left(\frac{2\dot{m}C}{WL}\right)T_{f2} = h_{cLf2}(T_{pv} - T_{f2}) + h_{cRf2}(T_R - T_{f2}) \quad (4)$$

Reflector

$$I_R = U_r(T_R - T_{amb}) + h_{cRf2}(T_R - T_{f2}) - h_{rLR}(T_L - T_R) \quad (5)$$

Where,

$$U_t = h_w + h_{rgs}$$

$$U_b = \frac{k_{ins}}{t_{ins} + h_w}$$

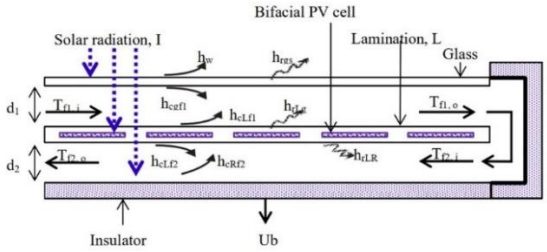

Fig. 2 Design a double-pass B-PVT collector with indicated heat transfer coefficients.

Equations (1) to (5) describe the energy relations modelled as a one-dimensional heat transfer steady-state model across the five distinct sections of the B-PVT: the cover, fluids in the upper channel, PV laminate, fluids in the lower channel, and reflector. These equations account for three modes of heat transfer, namely convection, conduction (denoted by the subscript c) and radiation (denoted by subscript r), where h represents heat transfer coefficients for interactions with internal or external fluids.

The left-hand side (LHS) of each relation in equation (1) to (5) represents the energy contained within the material, originating from solar irradiation denoted by I, or the kinetic energy due to fluid temperature within the upper and lower airflow channels. The right-hand side (RHS) represents the heat transfer phenomena occurring at each section. For instance, the PV laminate contains energy originating from solar irradiation (at RHS of equation 3), I_{pv}, which is dissipated into the surrounding fluid by convection and radiation (at LHS of equation 3) as denoted by h_{cLf1}, h_{cLf2}, h_{rLg} and h_{rLR}, along with temperature changes induced by each heat transfer mode.

As the solar irradiance is received by the B-PVT, a portion of its irradiance is reflected and absorbed by components in each section before being transmitted to the next. This reduction in irradiance can be expressed as follows:

Cover : $I_g = \alpha I$

Bifacial PV : $I_{pv} = I\tau_g\alpha_{pv}PF(1 - \eta_{front}) + I\tau_g\tau_L\alpha_{pv}PF(1 - PF)\eta_R(1 - \eta_{rear})$

Reflector : $I_R = I(1 - PF)\tau_L\tau_g(1 - \eta_R)$

Note that the solar irradiance captured by the bifacial PV has two terms for its front and back side. Here, the extent to which the solar irradiance is passed through the PV panel is controlled by its packing factor (PF), where high packing factors represent tight packing of the PV cells, allowing less sunlight to pass through to be reflected on the module's backside.

b. Heat transfer coefficients

The radiative and convective heat transfer coefficients of the collector are determined through a comprehensive literature analysis. The convective heat transfer coefficients, sourced from studies by (Syakirah Nazri *et al.,* 2018) and (Mustapha, Fudholi, and Sopian 2020), are presented in equations (6) to (8)

$$h_w = 2.8 + 3.3v \quad (6)$$

$$h_c = \frac{kNu}{D_h} \quad (7)$$

$$D_h = \frac{4Wd}{2(W+d)} = \frac{4A}{2Wd} \quad (8)$$

Equation (6) represents the convective heat transfer coefficients h_w due to the external fluid (ambient wind), hence denoted by subscript w, and thus influenced by the velocity of the ambient wind. Conversely, equation (7) represents the convective heat transfer of the internal fluid h_c (airflow in the channels), which takes account of the fluid thermal conductivity k, as expressed in equation (14), and D_h denotes the hydraulic diameter of the channels.

In computing the convective heat transfer h_c in equation (7), a dimensionless quantity, the Nusselt number (Nu), denoting the ratio of total heat transfer to conductive heat transfer, is required. The fluid's Nusselt number is highly dependent on its state, as described by its Prandtl (Pr) and Reynold number (Re). The Prandtl number signifies the ratio of momentum diffusivity to thermal diffusivity in the fluid, while the Reynolds number describes the ratio of inertial forces to viscous forces in the fluid flow. The Nusselt numbers for regions of laminar, transitional, and turbulent flow are then as follows (Fudholi *et al.,* 2018):

I. Re < 2300

$$Nu = 5.4 + \frac{0.0019\left[\frac{RePrD_h}{L}\right]^{1.71}}{1.0.00563\left[\frac{RePrD_h}{L}\right]^{1.71}}$$

II. 2300 < Re < 6000

$$Nu = 0.116\left[\left(Re^{\frac{2}{3}} - 125\right) Pr^{\frac{1}{3}}\left(1 + \left(\frac{D_h}{L}\right)^{\frac{2}{3}}\right)\right]\left[\frac{\mu^{0.14}}{\mu_w}\right]$$

III. Re > 6000

$$Nu = 0.18Re^{\frac{4}{5}}Pr^{\frac{2}{5}}$$

Where,

$$Pr = \frac{\mu C}{k}$$

$$Re = \frac{\dot{m}D_h}{A\mu}$$

Heat radiation modes signify the heat radiated by bodies via electromagnetic radiation without the need for a material medium. The Stefan-Boltzmann law governs such thermal transfer where its characteristics are dependent on the emissivity of the body and are proportional to the fourth power of its absolute temperature. This relationship is related by the Stefan-Boltzmann constant as represented by equations (9) to (11).

$$h_{rgs} = \frac{\sigma\epsilon_g\left(T_g + T_s\right)\left(T_g^2 + T_s^2\right)\left(T_g - T_s\right)}{T_g - T_{amb}} \quad (9)$$

Where the sky temperature (T_s) is determined by (Swinbank 1963):

$$T_s = 0.0552T_{amb}^{1.5}$$

$$h_{rLg} = \frac{\sigma\left(T_g^2 + T_{pv}^2\right)\left(T_{pv} + T_g\right)}{\frac{1}{\epsilon_{pv}} + \frac{1}{\epsilon_g} - 1} \quad (10)$$

$$h_{rLR} = \frac{\sigma(T_R^2 + T_R^2)\left(T_R + T_g\right)}{\frac{1}{\epsilon_{pv}} + \frac{1}{\epsilon_r} - 1} \quad (11)$$

When computing heat transfer coefficients of convection, it is important to evaluate the physical properties of the fluid of interest within the airflow channels. It is assumed that the properties of air follow a linear temperature variation, as expressed by equations (12) through (15) (Fudholi *et al.,* 2019):

$$\text{Viscosity } (\mu) = [1.983 + 0.00184(T - 27)] \times 10^{-5} \quad (12)$$

$$\text{Specific heat } (C) = [1.0057 + 0.000066(T - 300)] \quad (13)$$

$$\text{Thermal conductivity } (k) = 0.0262 + 0.0000758(T - 300) \quad (14)$$

$$\text{Heat capacity of fluid } \left(\dot{Q}\right) = \dot{m}C\Delta T \quad (15)$$

Equation (15) provides the necessary mathematical representation used for later discussions on the heat capacity of the fluid, while fluid properties of viscosity, specific heat and thermal conductivity are all essential in computing fluid parameters, as shown previously.

c. *Simulation procedures*

Table 1 explains the geometric, thermal, and physical initial values that were applied in the simulation. The matrix inversion method in MATLAB software was used to solve the equations described previously. The simulation was constrained to fundamental optical principles to ensure the properties of materials remained logical and feasible, which governed the materials' interaction with solar radiation, and expressed as follows:

$$\alpha + \tau + \rho = 1 \quad (16)$$

These principles are crucial for maintaining accuracy throughout the simulation.

d. *Energy analysis*

This research has several objectives, including thermal energy and electrical energy. The formulas for each of these efficiencies, as well as the overall efficiency, are explained below. The B-PVT system used in this case study was a bifacial photovoltaic panel JAM72D30-540. Therefore, the electrical efficiency of the front and rear surfaces was added to determine the total electrical efficiency (η_{pv}). Variations in PV temperature were used to compute electrical efficiency (Florschuetz 1979):

$$\text{Electrical efficiency, } \eta_{pv} = \eta_{pv,front} + \eta_{pv,rear} \quad (17)$$

Where,

$$\eta_{pv,front} = PF\left[\eta_{ref}\left(1 - \beta\left(T_{pv} - T_{ref}\right)\right)\right] \quad (18)$$

and with a bifaciality of 70%,

$$\eta_{pv,rear} = 0.7\eta_{pv,front}$$

The thermal energy produced by the bifacial PV cells was carried by the mass of airflow passing through the system. This performance is denoted by its thermal efficiency determined by the difference in the absolute air temperatures at the input and output as shown in equation (19).

$$\text{Thermal efficiency, } \eta_{th} = \frac{\dot{m}C(T_o - T_{in})}{AI} \quad (19)$$

Table 1
The simulation's geometric, thermal, and physical values

Parameters	Numerical values
Width, W	2.42
Length, L	1.34
Upper channel, d_1	0.12
Lower channel, d_2	0.12
Reference electrical efficiency, η_{ref}	20.7%
Temperature coefficient, β	0.0045
Ambient temperature, T_{amb}	30
Ambient wind speed, v	4
Inlent temperature, T_{in}	30
Mass flow rate, $\dot{m}$	0.2
Solar irradiation, I	800
Solar panel packing factor, PF	0.66
Transmittance of cover, τ_g	0.85
Transmittance of laminate, τ_L	0.6
Transmittance of PV panel, τ_{pv}	0.04
Absorption of cover, α_g	0.05
Absorption of PV panel, α_{pv}	0.91
Absorption of reflector, α_r	0.9
Reflectance of cover, ρ_g	0.1
Reflectance of reflector, ρ_r	0.05
Emissivity of cover, ϵ_g	0.9
Emissivity of PV, ϵ_{pv}	0.95
Emissivity of reflector, ϵ_r	0.9
Thermal conductivity of insulator, k_{ins}	80

Thus, by combining both energy efficiencies, the total output energy efficiency can be expressed as follows:

$$\text{Total efficiency, } \eta_{PVT} = \eta_{pv} + \eta_{th} \quad (20)$$

2.2. Mathematical model validation: experiment

Validation of the developed mathematical model was performed against experimental data. The Indonesian city of Bandung was the site of the experiments. During the measurements, real-world environmental conditions were recorded throughout the day, including solar intensity and wind speed, using a pyranometer and anemometer, respectively. A DC fan was placed at the B-PVT intake, which introduces a controlled mass flow of air into the collector. The use of a flow meter measured the fan output speed controlled by a power regulator. A DHT22 sensor and K-type thermocouples were positioned at specific points to measure the temperature of the PV panel, the reflector and the air at its inlet and outlet. Figure 3 shows the temperatures at the PV cells and cover throughout December 10th 2023, showing the difference between the results of the mathematical model against the measured experimental data. For this particular test, a PF of 1.0 was employed along with a set mass flow $\dot{m}$ of 0.2 kg/s. The average measured ambient velocity v_{amb} was at 4 m/s, assumed as constant in the mathematical model. Using the estimated parameters of transmissivity, absorptivity, reflectance, and emissivity of the materials of the B-PVT, as shown in Table 1, inaccuracies for the PV temperature at 9.188% and the cover temperature at 6.812% are deemed acceptable. This value is seen as an improvement to a previous study that found a deviation error of 18% (Nikzad, Zamen, and Ahmadi, 2022).

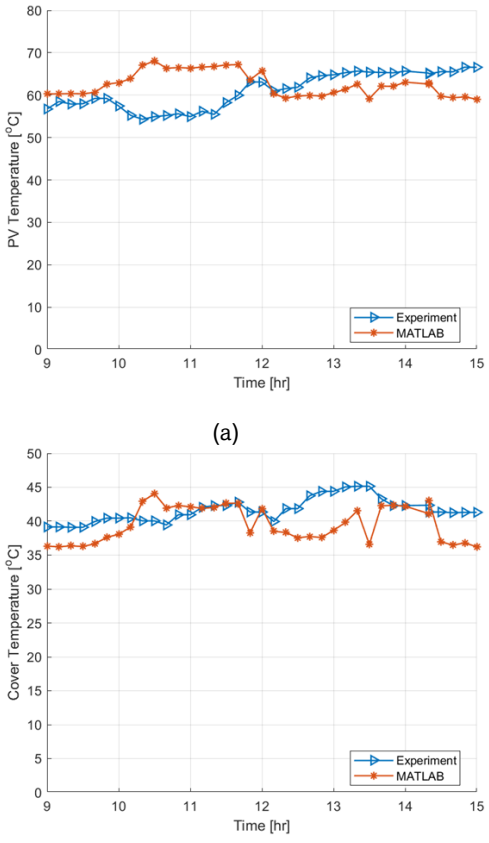

Fig. 3 Validation between experimental and mathematical models (a) PV temperature (b) cover temperature

3. Multi-objective optimization of B-PVT models

This section briefly discusses the optimization method used to complete the objectives of this study. In this study, the multi-objective problem of how components affect the output performance of air-based B-PVT systems is to be solved using the NSGA-II optimization approach.

3.1 Multi-objective optimization using NSGA-II

For this study, at least three conflicting objectives were analyzed. In previous literature studies, the Nondominated Sorting Genetic Algorithm (NSGA-II) has been commonly used for cases of two or more conflicting objectives (Yazdinejad *et al.*, 2023; Datta, Kapoor, and Mehta, 2023). In this case, it is mathematically described as the following equation (Deb 2001):

$$\begin{aligned} \text{Minimized} \quad & f_m(x), m = 1,2,\dots.,M; \\ \text{Subject to} \quad & g_j(x) \geq 0, j = 1,2,\dots.,J; \\ & h_k(x) = 0, k = 1,2,\dots.,K; \\ & x_i^{(L)} \leq x \leq x_i^{(U)}, i = 1,2,\dots.,n. \end{aligned} \quad (21)$$

With solution $\bar{x} = [x_1,\ x_2, \dots,\ x_n]$ to be a vector of dimension n, denoting the number of decision variables. In this particular case, the optimization is only subjected to linear equalities h_k, which is discussed in the latter subchapters, without any linear inequalities g_j. Superscripts (L) and (U) denotes the appropriate lower and upper boundaries for each choice variable.

Due to the complexity of the non-linearities within the B-PVT system, a metaheuristic evolutionary algorithm NSGA-II was implemented to get the optimal arrangement of design configurations. The algorithm started by initializing a set of samples, referred to as a population. Offsprings were produced

Table 2
NSGA-II tuning parameters

Parameter	Value
Population	200
Generations	100
Selection method	Tournament method
Mutation method	Adapt-feasible
Crossover fraction	0.8

from these samples according to crossover and mutation regulations. Subsequently, the B-PVT model assessed these two generations and arranged them according to their dominance and crowding distance within the objective space. We kept doing this until we reached convergence. The NSGA-II settings used in this work are listed in Table 2 and were judged appropriate for producing a high-quality final Pareto front. A collection of Pareto optimal solutions, or non-dominated solutions that cannot be improved without making at least one other objective function worse, is known as a Pareto front. This approach provides designers with choices and makes trade-offs within the set of optimal solutions without requiring them to consider every parameter range and combination.

3.2 The optimization problem

The three cases to be studied were divided into 2D and 3D optimizations. 2D and 3D optimization describes optimization between two objectives and three objectives, respectively. The trade-off between thermal and electrical efficiency is explained as Multi-Objective Problem 1 (MOP1). Next, the trade-off between temperature change ($\boldsymbol{\Delta T}$) and total efficiency is explained in MOP2. Finally, MOP3 is an optimization problem that examines the trade-off between the three outputs to achieve three objectives. As NSGA-II is designed for minimization, the objective functions were multiplied by a factor of (-1):

MOP 1:

$$\text{Minimize:} \quad f_1(\bar{x}) = -\eta_{th}, \quad f_2(\bar{x}) = -\eta_{PV} \tag{22}$$

MOP 2:

$$\text{Minimize:} \quad f_1(\bar{x}) = -\eta_{PVT} = -(\eta_{th} + \eta\_PV), \quad f_2(\bar{x}) = -\Delta T \tag{23}$$

MOP 3:

$$\text{Minimize:} \quad f_1(\bar{x}) = -\eta_{th}, \quad f_2(\bar{x}) = -\eta_{PV}, \quad f_3(\bar{x}) = -\Delta T \tag{24}$$

Sensible design parameters of the B-PVT system are identified with its components represented by the packing factor of PV cells, thermal insulators of the walls, and the absorption, transmittance and reflectance of the cover and reflector materials. Additionally, its configurations are represented by mass flow and channel depth ratio. Table 3 presents these initial decision variables, which the present work found to affect output performance. These variables will then be further reduced from the results of sensitivity analysis.

3.3 Reduction of decision variables

Design parameter variables which only have significant effects on the objective functions were selected for optimization in order to reduce the dimensionality of decision variables. This reduction is aimed to expedite the optimization process. The sensitivity and parametric analysis performed in sections 4.1 and 4.2 identifies these influential variables. With fewer decision variables, there exist fewer combinations to evaluate in obtaining the possible optimal solutions, particularly in multi-objective cases using non-gradient-based optimization algorithms, further reducing the computational requirement and solution times. These significant variables are then optimized while insensitive parameters are held constant in the search for optimal performance. The reduction of decision variables is thus as follows:

$$\bar{x} = [x_1, x_2, \dots, x_n] \rightarrow \bar{x}^r = [x_1, x_2, \dots, x_m]$$

Where $\boldsymbol{n} > \boldsymbol{m}$, with $\boldsymbol{n}$ and $\boldsymbol{m}$ denoting the number of variables, the superscript $\boldsymbol{r}$ denotes the reduced decision variables.

Table 3
Decision variables ($\bar{x}$) for multi-objective optimization problems

Symbols	Decision variable $\bar{x}$	Range
$\dot{m}$	Mass flow rate	$0.001 \leq x(1) \leq 0.2$
$\frac{d_1}{d_1 + d_2}$	Channel depth ratio of d_1	$0.1 \leq x(2) \leq 0.9$
PF	Packing factor	$0.1 \leq x(3) \leq 1$
α_g	Absorption of cover	$0.05 \leq x(4) \leq 0.95$
τ_g	Transmittance of cover	$0.05 \leq x(4) \leq 0.95$
ρ_g	Reflectance of cover	$0.01 \leq x(6) \leq 0.94$
τ_L	Transmittance of laminate	$0.5 \leq x(7) \leq 0.95$
α_r	Absorption of reflector	$0.05 \leq x(8) \leq 0.95$
ρ_r	Reflectance of reflector	$0.01 \leq x(9) \leq 0.94$
k_{ins}	Thermal conductivity of insulator	$0.12 \leq x(10) \leq 450$

4. Results and discussions

4.1 Mathematical models for parametric analysis

There are relatively many parameters that influence the defined objectives; this sub-chapter investigates the trends of objective parameters, namely electrical efficiency, thermal efficiency, and temperature differential. At least three independent parameter sweeps are presented, namely the

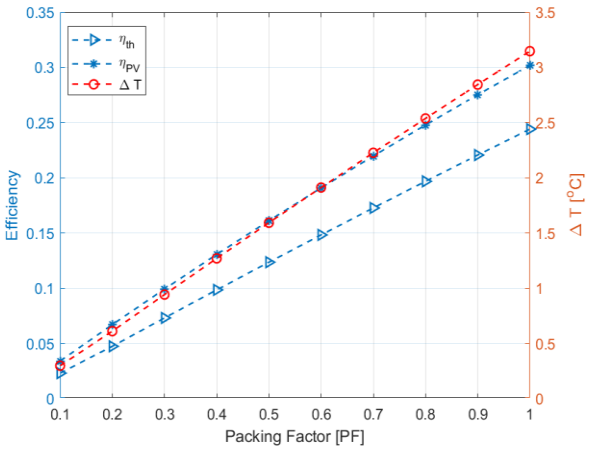

Fig. 4 The effect of the packing factor on $\boldsymbol{\eta_{th}, \eta_{PV}, and\ \Delta T}$

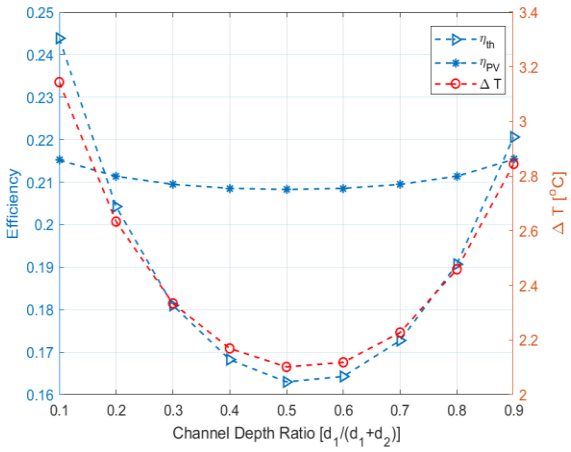

Fig. 5 Channel depth ratio vs $\boldsymbol{\eta_{th}, \eta_{PV}, and\ \Delta T}$

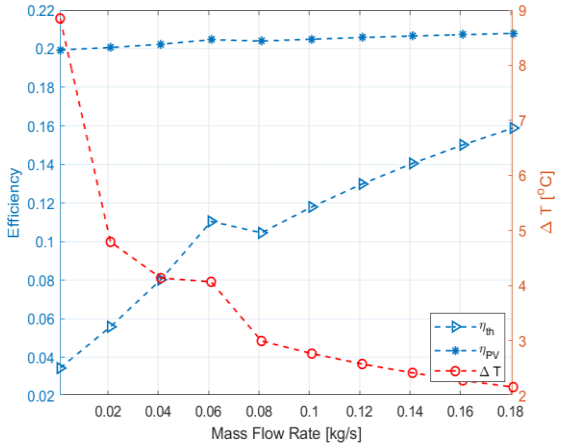

Fig. 6 Mass flow rate vs $\boldsymbol{\eta_{th}, \eta_{PV}, and\ \Delta T}$

packing factor, channel depth ratio, and mass flow rate. Figure 4 illustrates the effects of packing factors (PF) on the objectives.

From the graph in Figure 4, it is known that a higher PF yields a linearly increasing output for η_{th}, η_{PV}, and for ΔT. In the case of electrical efficiency, this is in accord with research by (Sehrawat *et al.*, 2022) and (Abbas *et al.*, 2022), who concluded that an increase of PF yields increasing electrical output as more of the panel is packed tight with PV cells for increased energy harvesting. However, the reference results mentioned above found that thermal efficiency decreases. This discrepancy in trends may be attributed to the difference in the PV cells used. In this study, the PV cells have high emissivity value ($\epsilon_{pv} = 0.95$) which facilitates a higher radiation heat transfer to the airflow, as seen in equation (10) and (11). With an increasing number of PV cells, i.e. higher PF, greater thermal energy was radiated away increasing the temperature of surrounding components. Therefore, the thermal energy can be indirectly carried away by the fluid through convection, thus increasing temperature differential and thermal efficiency.

Channel depth ratio is also a factor that was investigated as influencing PVT performance (Kumar and Dhiman 2022; Kumar and Dhiman 2023). Figure 5 shows the relationship between the channel depth ratio and the objectives discussed in this paper. From the graph in Figure 5, it is obtained that as the channel depth ratio deviated from 0.5, or the more asymmetry between the channel depths, the higher the thermal efficiency and delta temperature; however, this is not that significant for electrical efficiency. This phenomenon can be explained as follows: a decrease in one of the channel depths reduces the cross-sectional area (A), which results in a higher Reynolds number (Re) and Nusselt number (Nu), as seen in section 2.1(b). This condition, in turn, produces a higher convective heat transfer coefficient (h_c), as seen in equations (7) and (8), allowing greater thermal energy to be carried away by the fluid thus increasing the temperature differential and thus the thermal efficiency.

Additionally, it is evident that decreasing the upper channel depth relative to the lower channel might result in a higher thermal efficiency. This situation is due to the upper section receiving the bulk of solar irradiance that produces greater thermal energy required to be carried away. The lower section only received solar irradiance 'leaking' through the laminate of the PV cells; thus, the lower channel did not produce as much thermal energy as the upper channel. Therefore, decreasing the channel depth in the top channel will result in a more efficient rise in the convective heat transfer coefficient.

Equation (18) illustrates how the temperature of the PV cells (T_{pv}) was used to calculate electrical efficiency, the effect of differing channel depths did not have as significant an effect on its efficiency value. The PV cells underwent two modes of heat transfer, namely, convection and radiation. As a reduction in channel depths increases the convection ratio, it is evident that there is still a growing trend in electricity efficiency. However, since the radiation rate remained relatively unchanged (h_{rLg} and h_{rLR}), the overall electrical efficiency did not change significantly

Mass flow rate is also a theme that researchers in PVT systems often study. Figure 6 explains the relationship between mass flow rate, $\eta_{th}, \eta_{PV}, and\ \Delta T$. It is evident that when the flow rate increases, thermal and electrical efficiency rises. As was discovered in the preceding instance, a rise in convective heat transfer is responsible for the efficiency gain. However, in this case, higher Re and Nu numbers were brought about by an increase of mass flow. This situation allows greater thermal energy to be carried away, thus increasing the thermal efficiency. The slight increase in electrical efficiency is credited to the increased cooling effects, reducing the T_{pv} of the bifacial PV cells and therefore increasing its electrical efficiency, as seen in equation (17). This finding is in agreement with research conducted by (Xie *et al.*, 2024; Tiwari *et al.*, 2023b); however, changes in ΔT were not analyzed.

One major difference between the physical phenomenons presented in Figure 6 is that the temperature differential and thermal efficiency do not follow the same trend as found in Figure 5. This finding can be explained by the fluid's heat capacity acting as a heat transmission medium, as expressed in equation (15). Where $\dot{Q}$ is the heat energy, and C is the specific heat of the fluid as computed in equation (13). Within both cases, the increase in heat energy was brought about similarly due to the increase of convection. However, in the problem presented in Figure 5, the mass flow was kept constant; therefore $\dot{Q}$ is only a function of ΔT and vice versa. In the case of Figure 6, since mass flow varied, $\dot{Q}$ becomes a function of both $\dot{m}$ and ΔT. Therefore, for the same increase in $\dot{Q}$, a greater $\dot{m}$ would require less temperature differential ΔT. This phenomenon is evidenced in this particular case where an increase in thermal energy, and therefore thermal efficiency, was present. However, with higher mass flows, a necessity for a substantial temperature differential is less required. Consequently, the graph in Figure 6 shows a decreasing trend for ΔT.

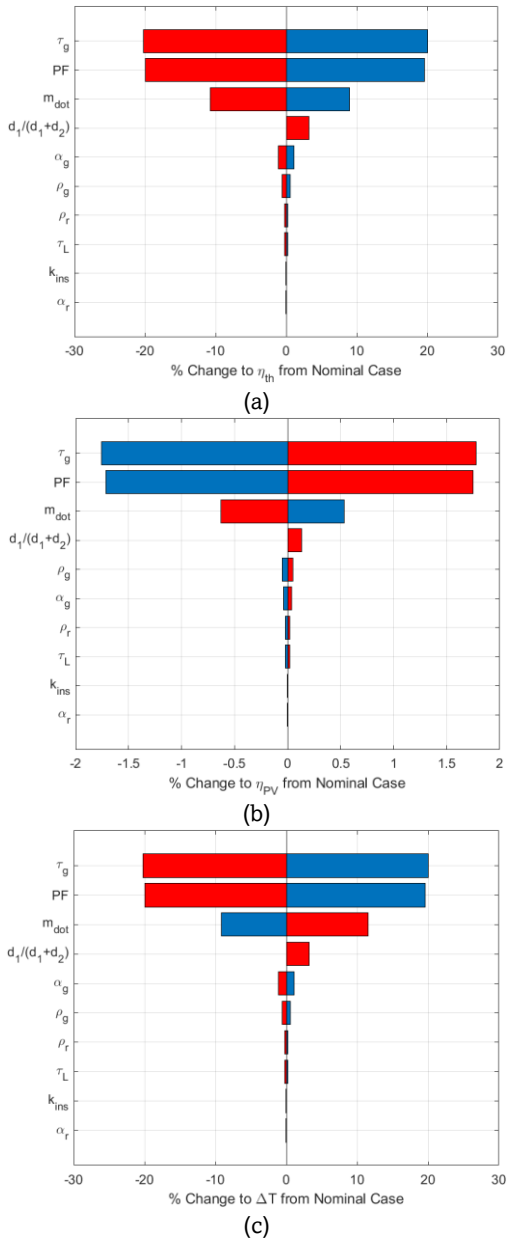

Fig. 7 Tornado plot of (a) thermal efficiency, (b) electrical efficiency (c) delta temperature

4.2 Sensitivity Analysis

This section investigates the rank of influence of each independent design variable towards each objective function to be then selected for optimization. Variables that do not have a great effect on the output can be removed without greatly affecting the final result. This reduction of the decision variables helps in reducing the computational power needed for the attainment of optimized solutions on the Pareto front.

Figure 7 is a tornado plot showing the extent to which each objective value deviates due to perturbation of each single design variable by $\pm\mathbf{20}\%$. Red-coloured bars indicate where the variable of interest is increased by 20%, while blue-coloured bars indicate the decrease of the variable value. It can be seen that different parameters have different magnitudes of effects on different objective values, each with its respective trends, where increasing a variable does not necessarily yield a favourable increase in objective performance.

From the tornado plots in Figures 7 (a), (b), and (c), the four variables that most influence thermal efficiency, electrical efficiency, and delta temperature are τ_g, PF, $\dot{m}$, and $\frac{d_1}{d_1+d_2}$. Figure 7 (a) can be read as follows: if $\dot{m}$ is reduced by 20% (e.g. between 1 and 0.8 m/s), it will result in a reduction in thermal efficiency of around 12%; if the $\dot{m}$ is added by 20% (e.g. starting 1 m/s to 1.2 m/s), it will result in an additional thermal efficiency of around 8%.

For thermal efficiency, as shown in Figure 7 (a), the cover transmissivity and packing factor can affect up to 20% and beyond. Figures 7 (a) and 7 (c) have the same trend, while for Figure 7 (b), transmissivity cover and packing factor are also the variables that most influence electrical efficiency, followed by mass flow rate and channel depth ratio, each around 1.8%, 0.6%, and 0.2%, respectively. From the graphs in the figure 7, it can be concluded that τ_L, α_r, ρ_r, and k_{ins}, have minimal effect on the objective functions of η_{th}, η_{PV}, and ΔT of this particular B-PVT system.

4.3 Optimization models

In this section, three multi-objective optimization cases are investigated: MOP1, MOP2 and MOP3. A metaheuristic NSGA-II algorithm was implemented to obtain optimal solutions for B-PVT design parameters. Constraints based on the fundamental optical principles governing the interaction of materials with solar radiation, as expressed in equation (16), were incorporated as linear equality constraints ($\boldsymbol{h_k}$) into the multi-objective optimization algorithm as depicted in equation (21).

For each MOP case, variables with dominant effects were selected for optimization. The sensitivity of the variables is presented in sub-chapter 4.2, specifically in Figure 7. From these figures, parameters that significantly affect the output of the B-PVT system can be identified. Table 4 summarizes the reduced decision variables to be optimized. In this research, the range of each respective decision variable was set as in the table. This step aims to restrict the solution space to produce results that are manufacturable and feasible.

a. 2D Plots

The trade-offs between the two distinct objectives were analyzed in the following 2D plots. By carrying out this 2D analysis, the trade-off relationship between objectives can be seen in more detail. This sub-chapter discusses two analyses

Table 4
Reduced decision variables ($\bar{\boldsymbol{x}}^{\boldsymbol{r}}$) for multi-objective optimization.

Symbols	Reduced decision variables $\bar{x}_{reduced}$	Range
$\dot{m}$	Mass flow rate	$0.001 \leq x(1) \leq 0.2$
$\frac{d_1}{d_1+d_2}$	Channel depth ratio of d_1	$0.1 \leq x(2) \leq 0.9$
PF	Packing factor	$0.1 \leq x(3) \leq 1$
α_g	Absorption of cover	$0.05 \leq x(4) \leq 0.95$
τ_g	Transmittance of cover	$0.05 \leq x(4) \leq 0.95$
ρ_g	Reflectance of cover	$0.01 \leq x(6) \leq 0.94$

Table 5
Optimized decision variables of MOP1

Design Variables	$\dot{m}$	$\frac{d_1}{d_1+d_2}$	PF	α_g	τ_g	ρ_g
$\bar{x}_0$(Nominal)	0.2	0.5	0.66	0.05	0.85	0.1
$\bar{x}_1^r$	0.197	0.129	0.999	0.623	0.356	0.020
$\bar{x}_2^r$	0.195	0.123	0.999	0.567	0.069	0.362
$\bar{x}_3^r$	0.194	0.111	0.999	0.053	0.051	0.895

that were carried out, namely Multi-Objective Problems 1 and 2 (MOP1 and MOP2).

The Pareto optimal solutions for the objective space MOP1 obtained through NSGA-II optimization using equation (22) are shown in Figure 8. These optimal solutions form the Pareto front, where an improvement in one objective produces a detrimental effect on the other. It can be seen that the nominal (initial) configuration, denoted by $\bar{x}_0$ and coloured in orange, does not lie within the Pareto front, thus indicating that by utilizing this configuration, the B-PVT system does not output its most optimal results. It is also apparent from the Figure 8 that electrical efficiency must fall as thermal efficiency rises. This finding is reliable with studies conducted by (Shojaeefard *et al.*, 2023), who found thermal and electrical efficiency with similar trends. Another study by (Zhao *et al.,* 2023) was carried out in Beijing. The average daily thermal efficiency can rise from 23.0% to 51.8% by increasing airflow, but the electrical efficiency only rises by roughly 3.5%. However, the optimization model in the present study does not only incorporate mass flow but other design configuration factors such as channel depths and material properties of the B-PVT cover previously not yet been investigated in available references. This finding expands the solution space, providing possible solutions with a greater number of different combinations of variables to produce further improved performance outputs.

Here, three sampling points of optimal solutions can be chosen with different weightage of the conflicting objectives to represent different user preferences. For example, if high electrical efficiency is required, $\bar{x}_3^r$ can be selected with an electrical efficiency value of around 34.17%. However, this option does not take into account the optimization of thermal efficiency, yielding only 4.29%, a thermal efficiency worse than yielded by the nominal configuration but with a much greater electrical efficiency. Conversely, if only high thermal efficiency is preferred, the $\bar{x}_1^r$ option can be selected, which increases the thermal efficiency to 34.54%, much higher than that yielded by the nominal configuration. Meanwhile, for a more balance preference, $\bar{x}_2^r$ can be selected, at this value, the electrical and thermal efficiency is 33.71% and 22.82%, respectively.

The optimized decision variables for each selected solution ($\bar{x}_0, \bar{x}_1^r, \bar{x}_2^r, \bar{x}_3^r$) are listed in Table 5. It is plain from the table that the following variables need to be met for optimal results of $\bar{x}_1^r$: The material properties of the cover are represented by α_g, τ_g, and ρ_g. The $\dot{m}$ should be 0.197, and the channel ratio by 0.129. Materials which closely match the parameters in the table should be found for the condition and optimal results of $\bar{x}_1$. Likewise, the same scheme is applicable to obtain optimal values of $\bar{x}_2^r$ and $\bar{x}_3^r$. It can be concluded that for the increased efficiency performance of this particular case, it is favourable to have high mass flow, with a great packing factor coupled with a reduction in the upper channel depth and less transmissibility in the cover. Intuitively, to maximize electrical efficiency, it is favoured to have higher transmissibility; however, in this case, the reduced transmissibility is obtained due to the optimization model favouring a maximization of thermal efficiency where greater reflectivity and absorptivity (better emissivity) increases the temperature of the cover and thus greater thermal energy transferred to the fluid.

The Pareto optimal solutions for MOP2 obtained through NSGA-II optimization using equation (23) are shown in Figure 9, which also shows the trade-off relationship between the temperature differential and the Total Efficiency $\boldsymbol{\eta_{PVT}}$ objective. As previously, it can be seen that the nominal (initial) configuration does not provide optimal output as it does not lie within the Pareto front. Three sample points with different weightages between the two objectives can be chosen to be analyzed.

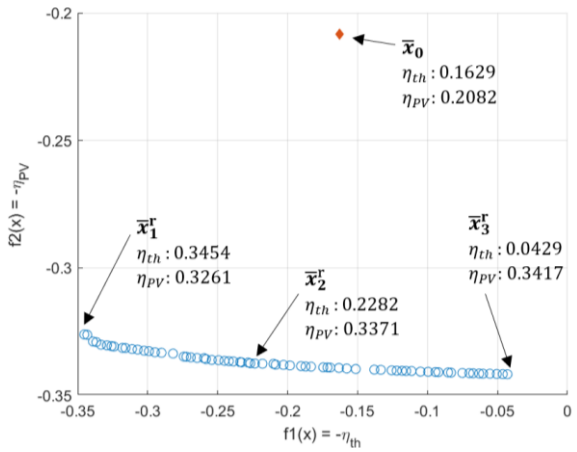

Fig. 8 Pareto-optimal outcomes in MOP1 objective space

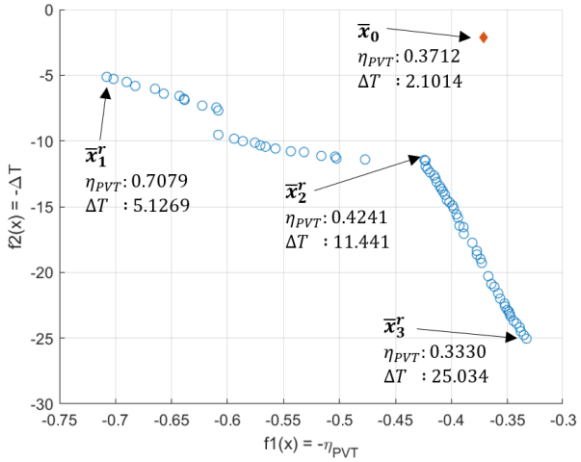

Fig. 9 Pareto-optimal outcomes in MOP2 objective space

Table 6
Optimized decision variable of MOP 2.

Design Variables	$\dot{m}$	$\frac{d_1}{d_1+d_2}$	PF	α_g	τ_g	ρ_g
$\bar{x}_0$(Nominal)	0.2	0.5	0.66	0.05	0.85	0.1
$\bar{x}_1^r$	0.197	0.107	0.997	0.148	0.841	0.010
$\bar{x}_2^r$	0.030	0.106	0.997	0.129	0.860	0.010
$\bar{x}_3^r$	0.005	0.115	0.997	0.112	0.876	0.010

Option $\bar{x}_3^r$, where the exit air temperature rises by roughly 25.03 degrees Celsius from the inlet air temperature, can be selected for air-based B-PVT applications that require high-temperature output. However, this particular solution yields a relatively poor total efficiency, which is unfavourable. Option $\bar{x}_3^r$, which has a total efficiency score of 70.79%, is an option for high total efficiency. The solution $\bar{x}_2^r$ represent a more balanced weightage of an optimal solution, which is 42.41% for overall efficiency and 11.44 degrees Celsius for temperature differential.

It is clear from looking at the trade-off relationship of optimal solutions that when the temperature differential rises, overall efficiency falls. The link between these two goals was not particularly addressed in previous research on liquid amorphous silicon solar photovoltaic thermal (PVT) air collectors (SPVTAC). According to earlier studies, for every degree increase in the intake temperature, the thermal efficiency of amorphous silicon SPVTAC reduced by around 0.45%, the electrical efficiency decreased by about 0.042%, and the temperature difference between the inlet and output decreased by 0.24 °C. (Huang *et al.,* 2021).

Table 6 summarises the optimized decision variables for each selected solution ($\bar{x}_1^r, \bar{x}_2^r, \bar{x}_3^r$). Similarly, as explained earlier, the material properties of the cover are represented by α_g, τ_g, and ρ_g with design configurations represented by $\dot{m}$, $\frac{d_1}{d_1+d_2}$ and PF. The specification values for each component affecting ΔT and total efficiency can be selected according to the desired design variable. It can be concluded that for increased overall efficiency performance, a greater mass flow is favourable; however, the opposite was found when a greater temperature differential is desired.

In MOP2, it was also found that the optimization favours high transmissibility amongst other design variables, which is a major difference from that found in the MOP1 case. This finding may be attributed due to the form of the objective function for the overall efficiency ($\eta_{PVT} = \eta_{th} + \eta_{pv}$) where both thermal and electrical efficiency have equal weightage; therefore, both objectives are maximized equally. In MOP1, the thermal efficiency objective mostly dominates the electrical efficiency objective; thus lower transmissibility is preferred as that would increase the heat radiating from the cover. Using the different forms of the objective function in MOP2, therefore, yields solutions where greater transmissibility of the cover is equally important to the maximization of electrical efficiency.

b. 3D Plots

In this 3D plot, the trade-off relationship between three conflicting objectives is analyzed, and this includes thermal efficiency, electrical efficiency, and temperature differential. The Pareto optimal solutions from the resulting optimization between these three objectives are depicted in Figure 10 below.

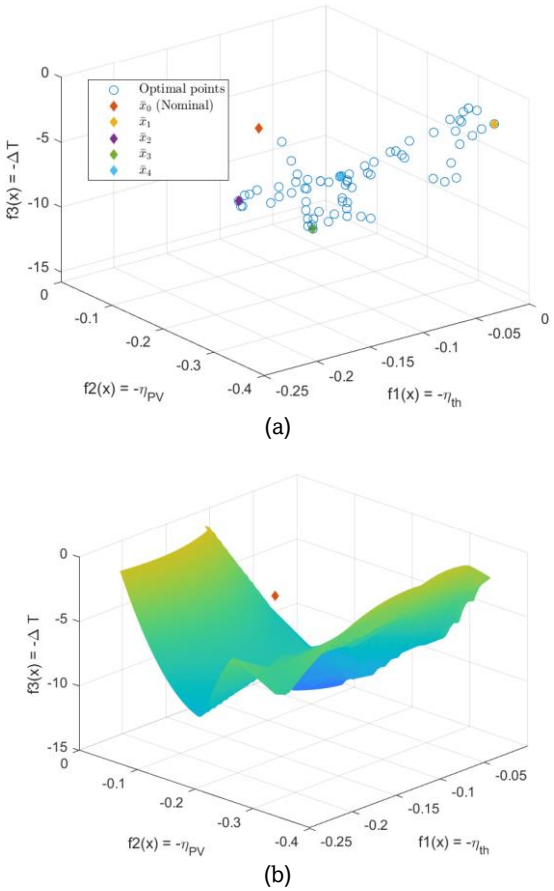

Fig. 10 Pareto-optimal outcomes in MOP3 objective space (a) Pareto optimal solutions (b) Pareto surface

To make the Pareto optimal solutions in the MOP3 objective space obtained through NSGA-II optimization using equation (24) that is shown in Figure 10 easier to analyze, Table 7 presents the optimal solutions from each chosen sample point. Every sample point is distinct from the others and operates independently. As previously, the nominal (initial) configuration does not provide optimal output as it does not lie within the Pareto surface thus indicating an inefficient configuration of the B-PVT system. With a gain of up to 33.77%, point $\bar{x}_1^r$ exhibits the maximum electrical efficiency, while point $\bar{x}_2^r$ has the best thermal efficiency, at 21.83%. The greatest ΔT and balance are displayed, respectively, at points $\bar{x}_3^r$ and $\bar{x}_4^r$.

The values in accordance with the points delineated in Table 7 and Figure 10 can next be examined in more detail. Table 8 shows the optimised decision variables for each component,

Table 7
Sample point values of the Pareto-optimal outcome in MOP 3

Design Variables	Thermal Efficiency (η_{th})	Electrical Efficiency (η_{PV})	Temperature Difference (ΔT)
$\bar{x}_0$ (Nominal)	16,30%	20,83%	2.10 °C
$\bar{x}_1^r$	0,31%	33,77%	2.96 °C
$\bar{x}_2^r$	21,83%	28,34%	5.10 °C
$\bar{x}_3^r$	3,20%	4,11%	15.78 °C
$\bar{x}_4^r$	10,87%	25,68%	6.10 °C

which significantly affects the output performance of the air-based B-PVT system. For example, in a situation where a B-PVT system with high thermal efficiency ($\bar{x}_2^r$) is required, its configuration is expected to have the ability to modify to the following values: $\dot{m}$ = 0.11030, $\frac{d_1}{d_1+d_2}$ = 0.16, PF = 0.88 , α_g= 0.60, τ_g=0.35 and ρ_g= 0.05. Similarly, each component's parameters can be looked up based on the needs of users accordingly, with different importance between the three objectives.

It is also important to note the differences in objective functions and how it yields different solutions. For example, in the case of MOP3, it is found that the highest possible performance of thermal efficiency is at 21.83% with electrical efficiency and temperature differential of 28.34% and 5.10°C, respectively. Taking a similar case for MOP1, it is found that the highest possible performance in thermal efficiency is at 34.54% with an electrical efficiency of 32.61% (with this solution, the particular configuration was found to yield a ΔT of 4.5°C). This discrepancy is attributed to the ΔT objective considered in MOP3, thus restricting the solutions and variable combinations produced by the optimization algorithm. As ΔT was not considered in MOP1, a lower ΔT value was yielded, which may not be sufficient enough to use in certain real-world applications of B-PVT.

As different optimization approaches yield different solutions, it is then imperative that users take careful considerations when choosing appropriate objective function(s) and optimal solution points that yield the desired output performance(s). The different choices may be in different forms of each objective function and/or the combinations and number of conflicting objectives and not restricted to only those presented in this study.

In all 2D and 3D cases, any point on the Pareto front or Pareto surface is its most optimal solution, where increasing one objective would require sacrificing other objectives. Therefore, the choice falls solely to the user and their external design requirements of the output performance needed from the B-PVT system. Achieving the theoretical optimal output of the B-PVT system is performed by setting design configurations and material properties as produced by the optimisation algorithm. From the present solutions, optimal points were found to improve in all objectives, solutions which would be difficult to obtain via simple parameter sweeps due to the coupling and non-linearities of different physical phenomena, thus supporting the use of NSGA-II as the optimisation algorithm.

5. Conclusion and Recommendation

The present study has identified and examined significant design parameters to their performance efficiencies of the B-PVT system and has provided an optimisation framework using NSGA-II in maximising the potential optimal performance. Sensitivity and parametric analysis were conducted to produce a rank of influence of independent design variables towards the objectives to be selected for optimization. It was found that higher backing factors contribute to improved thermal and electrical efficiencies alongside increased temperature differential. A similar effect can be found with asymmetry in channel depths. However, higher mass flows correlate to increased thermal and electrical efficiencies while reducing temperature differential.

Sensitivity analysis identified key design variables with significant influences on the output performances of the B-PVT system. It was found that variables of cover transmissivity, packing factors and channel depth ratios have influential effects on objective performances. For instance, the cover transmissivity and packing factors have been found to have an impact of magnitudes up to 20% on thermal efficiency and temperature differentials, while mass flow rates and channel depth ratios have their most influential effects on electrical efficiencies of around 0.2-1.8%. This finding establishes the key parameters contributing to B-PVT performance. Insignificant parameters could then be kept constant at their nominal values for the purposes of optimization, allowing for faster convergence towards optimal solutions.

The multi-objective optimization produces a distinct Pareto front of non-dominating optimal solutions between conflicting objectives. The set of these optimal points represents various weight preferences towards the maximization of different objectives, where each denotes a particular B-PVT configuration with different combinations of design variables. NSGA-II facilitates the attainment of these optimal solutions, as

Table 8
Optimized decision variable of MOP3.

Design Variables	$\dot{m}$	$\frac{d_1}{d_1+d_2}$	PF	α_g	τ_g	ρ_g
$\bar{x}_0$ (Nominal)	0.2	0.5	0.66	0.05	0.85	0.1
$\bar{x}_1^r$	0.002	0.100	0.999	0.050	0.050	0.899
$\bar{x}_2^r$	0.110	0.160	0.880	0.598	0.347	0.054
$\bar{x}_3^r$	0.005	0.115	0.127	0.913	0.076	0.010
$\bar{x}_4^r$	0.045	0.127	0.787	0.472	0.224	0.303

simple parameter sweeps for optimization would have been difficult due to the complex nature of the coupled physical phenomenon between heat transfer modes.

Nominal (initial) design parameter values, as shown in Table 1, were found to have a non-optimal output performance in thermal electrical efficiencies as well as temperature differential. Its location on the objective space indicates this as these values were not found on the Pareto front or Pareto surface indicating that the B-PVT system could be further optimized for maximizing output performance.

An analysis of the trade-off relationship between optimal solutions of electrical efficiency and thermal efficiency: MOP1 of equation (22), a greater preference for performance in electrical efficiency, less preference must be allocated to thermal efficiency. For example, a preference only towards electrical efficiency yields an optimal value of around 34.17%, with relatively poor performance of thermal efficiency of only 4.29%, lower than the performance of thermal efficiency yielded by the nominal configuration. In contrast, an optimal solution may be chosen with more preference towards thermal efficiency to greatly improve the thermal performance, however, at the expense of electrical efficiency. Each solution on the Pareto front provides users with distinct B-PVT configurations to choose from.

On the trade-off relationship between the temperature differential and the total efficiency, MOP2 of equation (23) offers a different perspective by optimizing the B-PVT system between different objective functions as previously. Here, a balanced weight of preferences of the optimal solutions could yield up to 42.41% for overall efficiency and 11.44 degrees Celsius for temperature differential. However, if user requirements restrict certain performance outputs, other optimal solutions may be selected accordingly. Solutions with increased overall efficiency were found to have a poor temperature differential and vice versa.

Based on analysing the trade-off relationship between thermal efficiency, electrical efficiency, and temperature differential conflicting objectives, MOP3 of equation (24), the same principle applies where the Pareto surface represents a set of optimal solutions where an increase in one objective is at the expense of the others. For example, in the case where a B-PVT system with only high thermal efficiency is required, its configuration is expected to have the ability to be modified to the following values: $\dot{m} = 0.11030$, $\frac{d_1}{d_1+d_2} = 0.16$, $PF = 0.88$, $\alpha_g = 0.60$, $\tau_g = 0.35$ and $\rho_g = 0.05$. This configuration would yield a relatively high thermal efficiency of 21.83% with poor performances in other objectives.

It is also important to note that the highest weightage of thermal efficiency in MOP3 does not yield as high as the optimal performance of MOP1 ($\eta_{th} = 34.54\%$). This finding is due to the added consideration of ΔT objective not present in MOP1, which restricts the optimal solutions of MOP3. These different approaches must be considered by users when optimizing a B-PVT system to identify the appropriate objective functions for the desired output performance of its solutions.

The present study is presented as a foundation to support future studies in further investigating other variables in material qualities, system configurations and operations under environmental uncertainty. Different approaches in modelling and optimizing such B-PVT systems may be implemented in place of the proposed approach in this study. Approaches such as machine learning surrogate modelling could be used in place of physics-based models, which could capture the complex physical nature, leading to greater PVT performance prediction and design improvements. Recursive parameter estimation of B-PVT parameters based on real-time data measurements could also enable dynamic optimization, providing continuous optimal configuration adjustments under changing environments.

Acknowledgements

The authors would like to express their gratitude to Universiti Teknologi Malaysia (UTM), Johor Bahru, Malaysia, and Badan Riset dan Inovasi Nasional (BRIN), Bandung, Indonesia, for facilitating all of the data gathering and supplying sophisticated literature on the completion of this work. Also acknowledged are all UTM instructors, BRIN researchers, staff members, and research assistants who contributed to the success of this project.

Author Contributions: All authors contributed equally as the main contributors to this paper. The final paper was read and approved by all authors.

Funding: This work was carried out under the auspices of the Badan Riset Inovasi Nasional, Indonesia (BRIN) and Universiti Teknologi Malaysia (UTM) Collaborative Research Grant vot R.J130000.7351.4B734.

References

Abbas, S., Yuan, Y., Zhou, J., Hassan, A., Yu, M., & Yasheng, J. (2022). Experimental and analytical analysis of the impact of different base plate materials and design parameters on the performance of the photovoltaic/thermal system. *Renewable Energy*, *187*, 522-536. https://doi.org/10.1016/j.renene.2022.01.088

Abdul-Ganiyu, S., Quansah, D. A., Ramde, E. W., Seidu, R., & Adaramola, M. S. (2021). Study effect of flow rate on flat-plate water-based photovoltaic-thermal (PVT) system performance by analytical technique. *Journal of Cleaner Production*, *321*, 128985. https://doi.org/10.1016/j.jclepro.2021.128985

Abdulmajeed, O. M., Jadallah, A. A., Bilal, G. A., & Arıcı, M. (2022). Experimental investigation on the performance of an advanced bi-fluid photovoltaic thermal solar collector system. *Sustainable Energy Technologies and Assessments*, *54*, 102865. https://doi.org/10.1016/j.seta.2022.102865

An, B. H., Choi, K. H., & Choi, H. U. (2022). Influence of triangle-shaped obstacles on the energy and exergy performance of an air-cooled photovoltaic thermal (PVT) collector. *Sustainability*, *14*(20), 13233. https://doi.org/10.3390/su142013233

Choi, Y. (2022). Seasonal Performance Evaluation of Air-Based Solar Photovoltaic/Thermal Hybrid System. *Energies*, *15*(13), 4695. https://doi.org/10.3390/en15134695

Datta, S., Kapoor, R., & Mehta, P. (2023). A multi-objective optimization model for outpatient care delivery with service fairness. *Business Process Management Journal*, *29*(3), 630-652. https://doi.org/10.1108/BPMJ-07-2022-0335

Deb, K. (2001). *Multi-objective optimization using evolutionary algorithms* (Vol. 16). John Wiley & Sons.

Ewe, W. E., Sopian, K., Mohanraj, M., Fudholi, A., Asim, N., & Ibrahim, A. (2024). Exergetic performance of jet impingement bifacial photovoltaic-thermal solar air collector with different packing factors and jet distributions. *Heat Transfer Engineering*, *45*(10), 904-914. https://doi.org/10.1080/01457632.2023.2227807

Florschuetz, L. W. (1979). Extension of the Hottel-Whillier model to the analysis of combined photovoltaic/thermal flat plate collectors. *Solar energy*, *22*(4), 361-366. https://doi.org/10.1016/0038-092X(79)90190-7

Fudholi, A., Zohri, M., Jin, G. L., Ibrahim, A., Yen, C. H., Othman, M. Y., ... & Sopian, K. (2018). Energy and exergy analyses of photovoltaic thermal collector with∇-groove. *Solar Energy*, *159*, 742-750. https://doi.org/10.1016/j.solener.2017.11.056

Fudholi, A., Zohri, M., Rukman, N. S. B., Nazri, N. S., Mustapha, M., Yen, C. H., ... & Sopian, K. (2019). Exergy and sustainability index of photovoltaic thermal (PVT) air collector: A theoretical and experimental study. *Renewable and Sustainable Energy*

Reviews, *100*, 44-51. https://doi.org/10.1016/j.rser.2018.10.019

Gopi, S., & Muraleedharan, C. (2022). Modelling and experimental studies on a double-pass hybrid photovoltaic-thermal solar air heater with vertical slats attached in the lower channel. *International Journal of Ambient Energy*, *43*(1), 4664-4674. https://doi.org/10.1080/01430750.2021.1918241

Gürbüz, E. Y., Kusun, B., Tuncer, A. D., & Ural, T. (2023). Experimental investigation of a double-flow photovoltaic/thermal air collector with natural dolomite powder-embedded thermal energy storage unit. *Journal of Energy Storage*, *64*, 107220. https://doi.org/10.1016/j.est.2023.107220

Hamada, A., Emam, M., Refaey, H. A., Moawed, M., & Abdelrahman, M. A. (2023). Investigating the performance of a water-based PVT system using encapsulated PCM balls: An experimental study. *Energy*, *284*, 128574. https://doi.org/10.1016/j.energy.2023.128574

Huang, M., Wang, Y., Li, M., Keovisar, V., Li, X., Kong, D., & Yu, Q. (2021). Comparative study on energy and exergy properties of solar photovoltaic/thermal air collector based on amorphous silicon cells. *Applied Thermal Engineering*, *185*, 116376. https://doi.org/10.1016/j.applthermaleng.2020.116376

Ishak, M. A. A. B., Ibrahim, A., Fauzan, M. F., Fazlizan, A., Ewe, W. E., & Kazem, H. A. (2023). The effect of a reversed circular jet impingement on a bifacial module PVT collector energy performance. *Case Studies in Thermal Engineering*, *52*, 103752. https://doi.org/10.1016/j.csite.2023.103752

Kallio, S., & Siroux, M. (2020). Energy analysis and exergy optimization of photovoltaic-thermal collector. *Energies*, *13*(19), 5106. https://doi.org/10.3390/en13195106

Kumar, A., & Dhiman, P. (2022). Analytical and experimental investigations of recyclic double pass photovoltaic thermal system. *Energy Sources, Part A: Recovery, Utilization, and Environmental Effects*, *44*(1), 669-684. https://doi.org/10.1080/15567036.2022.2048924

Kumar, A., & Dhiman, P. (2023). Modeling and optimization of photovoltaic thermal system under recyclic operation by response surface methodology. *Renewable Energy*, *203*, 228-244. https://doi.org/10.1016/j.renene.2022.12.053

Li, Z. X., Shahsavar, A., Al-Rashed, A. A., Kalbasi, R., Afrand, M., & Talebizadehsardari, P. (2019). Multi-objective energy and exergy optimization of different configurations of hybrid earth-air heat exchanger and building integrated photovoltaic/thermal system. *Energy Conversion and Management*, *195*, 1098-1110. https://doi.org/10.1016/j.enconman.2019.05.074

Mustapha, M., Fudholi, A., Nazri, N. S., Zaini, M. I. A., Rosli, N. N., Sulong, W. M. W., & Sopian, K. (2023). Mathematical modeling and experimental validation of bifacial photovoltaic–thermal system with mirror reflector. *Case Studies in Thermal Engineering*, *43*, 102800. https://doi.org/10.1016/j.csite.2023.102800

Fudholi, A., & Mustapha, M. (2020). Mathematical modelling of bifacial photovoltaic-thermal (BPVT) collector with mirror reflector. *International Journal of Renewable Energy Research (IJRER)*, *10*(2), 654-662. https://doi.org/10.20508/ijrer.v10i2.10603.g7936

Nazri, N. S., Fudholi, A., Mustafa, W., Yen, C. H., Mohammad, M., Ruslan, M. H., & Sopian, K. (2019). Exergy and improvement potential of hybrid photovoltaic thermal/thermoelectric (PVT/TE) air collector. *Renewable and Sustainable Energy Reviews*, *111*, 132-144. https://doi.org/10.1016/j.rser.2019.03.024

Nikzad, M., Zamen, M., & Ahmadi, M. H. (2022). Theoretical and experimental investigation of a photovoltaic/thermal panel partially equipped with thermoelectric generator under unstable operating conditions. *International Journal of Energy Research*, *46*(5), 6790-6805. https://doi.org/10.1002/er.7621

Podder, B., Das, S., & Biswas, A. (2023). Numerical analysis of a small sized water based solar photovoltaic-thermal collector. *International Journal of Green Energy*, *20*(2), 113-128. https://doi.org/10.1080/15435075.2021.2023881

Rajani, A., Darussalam, R., Pramana, R. I., & Santosa, A. (2018, November). Simulation of PV-Biogas Integration on hybrid power plant using HOMER: Study case of superior livestock breeding center and forage of animal feed (bbptu-hpt) baturraden. In *2018 International Conference on Sustainable Energy Engineering and Application (ICSEEA)* (pp. 69-74). IEEE. https://doi.org/10.1109/ICSEEA.2018.8627132

Ranjan, A., Podder, B., Das, B., & Biswas, A. (2024). Computational investigation of an innovative solar photovoltaic thermal collector with spiral shaped absorber using bifluid coolant. *International Journal of Environmental Science and Technology*, *21*(3), 2827-2842. https://doi.org/10.1007/s13762-023-05088-0

Sehrawat, R., Sahdev, R. K., Tiwari, S., Sehrawat, P., & Kumar, A. (2022, December). Recent advancements on Photovoltaic thermal and Greenhouse Dryer. In *2022 International Conference on Computational Modelling, Simulation and Optimization (ICCMSO)* (pp. 374-378). IEEE. https://doi.org/10.1109/ICCMSO58359.2022.00078

Shojaeefard, M. H., Al-Hamzawi, H. A. H., & Sharfabadi, M. M. (2023). Evaluating the Performance of Photovoltaic Thermal Systems in Varied Climate Conditions: An Exergy and Energy Analysis Approach. *International Journal of Heat & Technology*, *41*(6). https://doi.org/10.18280/ijht.410610

Su, W., Lu, Z., She, X., Zhou, J., Wang, F., Sun, B., & Zhang, X. (2022). Liquid desiccant regeneration for advanced air conditioning: A comprehensive review on desiccant materials, regenerators, systems and improvement technologies. *Applied Energy*, *308*, 118394. https://doi.org/10.1016/j.apenergy.2021.118394

Swinbank, W. C. (1963). Long-wave radiation from clear skies. *Quarterly Journal of the Royal Meteorological Society*, *89*(381), 339-348. https://doi.org/10.1002/qj.49708938105

Nazri, N. S., Fudholi, A., Ruslan, M. H., & Sopian, K. (2018). Mathematical modeling of photovoltaic thermal-thermoelectric (PVT-TE) air collector. *International Journal of Power Electronics and Drive Systems (IJPEDS)*, *9*(2), 795-802. https://doi.org/10.11591/ijpeds.v9.i2.pp795-802

Vera, J. T., Laukkanen, T., & Sirén, K. (2014). Performance evaluation and multi-objective optimization of hybrid photovoltaic–thermal collectors. *Solar energy*, *102*, 223-233. https://doi.org/10.1016/j.solener.2014.01.014

Vera, J. T., Laukkanen, T., & Sirén, K. (2014). Multi-objective optimization of hybrid photovoltaic–thermal collectors integrated in a DHW heating system. *Energy and Buildings*, *74*, 78-90. https://doi.org/10.1016/j.enbuild.2014.01.011

Tiwari, A. K., Chatterjee, K., & Deolia, V. K. (2023). Application of copper oxide nanofluid and phase change material on the performance of hybrid photovoltaic–thermal (PVT) system. *Processes*, *11*(6), 1602. https://doi.org/10.3390/pr11061602

Tiwari, A. K., Chatterjee, K., & Deolia, V. K. (2023). Effect of mass flow rate on the thermo-electrical performance of hybrid PVT system with curved-groove absorber. *Journal of the Brazilian Society of Mechanical Sciences and Engineering*, *45*(7), 382. https://doi.org/10.1007/s40430-023-04279-7

Urrejola, E., Antonanzas, J., Ayala, P., Salgado, M., Ramírez-Sagner, G., Cortés, C., ... & Escobar, R. (2016). Effect of soiling and sunlight exposure on the performance ratio of photovoltaic technologies in Santiago, Chile. *Energy Conversion and Management*, *114*, 338-347. https://doi.org/10.1016/j.enconman.2016.02.016

Xie, Y., Zhou, J., Bisengimana, E., Jiang, F., Ji, W., Sun, L., ... & Yuan, Y. (2024). Exergy performance assessment of a novel air-cooled photovoltaic thermal collector with a double serpentine runner. *Applied Thermal Engineering*, *236*, 121330. https://doi.org/10.1016/j.applthermaleng.2023.121330

Yazdinejad, A., Dehghantanha, A., Parizi, R. M., & Epiphaniou, G. (2023). An optimized fuzzy deep learning model for data classification based on NSGA-II. *Neurocomputing*, *522*, 116-128. https://doi.org/10.1016/j.neucom.2022.12.027

Youns, Y. T., & Manshad, A. K. (2023). Effect of Green Nanomaterials on CO2 Diffusion Coefficient and Interfacial Tension in Nanofluids: Implication for CO2 Sequestrations. *Arabian Journal for Science and Engineering*, 1-29. https://doi.org/10.1007/s13369-023-08551-9

Zarei, A., Izadpanah, E., & Babaie Rabiee, M. (2023). Using a nanofluid-based photovoltaic thermal (PVT) collector and eco-friendly refrigerant for solar compression cooling system. *Journal of Thermal Analysis and Calorimetry*, *148*(5), 2041-2055. https://doi.org/10.1007/s10973-022-11850-2

Zhao, Y., Li, W., Zhang, G., Li, Y., Ge, M., & Wang, S. (2023).

Experimental performance of air-type BIPVT systems under different climate conditions. *Sustainable Energy Technologies and Assessments*, *60*, 103458. https://doi.org/10.1016/j.seta.2023.103458